UNIVERSITY OF BIRMINGHAM
University of Birmingham Research at Birmingham

Orientational selective growth of single-atomic-layer gold nano-sheet via van der Waals interlocking and octanethiolate-confined molecular channels

Zhang, Xin; Gao, Jianzhi; Fan, Xing; Wang, Yitao; Ding, Haoxuan; Qin, Xuhui; Jiang, Shuhang; Zhao, Tiantian; Zhu, Gangqiang; Lu, Hongbing; Yang, Zhibo; Lin, Haiping; Li, Qing; Chi, Lifeng; Pan, Minghu; Guo, Quanmin

Document Version
Peer reviewed version

Link to publication on Research at Birmingham portal

Download date: 04. May. 2024

Orientation-selective growth of rectangular gold sheets via van der Waals interlocking

Xin Zhang[1,†], Jianzhi Gao[2†], Yitao Wang[3], Haoxuan Ding[3], Xuhui Qin[2], He Bai[2], Tiantian Zhao[2] , Gangqiang Zhu[2], Hongbing Lu[2], Zhibo Yang[2], Haiping Lin[4], Qing Li[4], Lifeng Chi[4,*], Minghu Pan[1,*], Quanmin Guo[3,*]

[1]School of Physics, Huazhong University of Science and Technology, Wuhan 430074, China.

[2]School of Physics and Information Technology, Shaanxi Normal University, Xi'an 710119, China.

[3]School of Physics and Astronomy, University of Birmingham, Birmingham, B15 2TT, United Kingdom.

[4]Institute of Functional Nano & Soft Materials, Jiangsu Key Laboratory for Carbon-Based Functional Materials & Devices, Collaborative Innovation Center of Suzhou Nano Science and Technology, Soochow University, 199 Ren-Ai Road, Suzhou, Jiangsu Province, 215123, China.

ABSTRACT:

Rectangular gold nano-sheets have been synthesized on the Au(111) substrate guided by an octanethiolate (OT) surfactant, in great contrast to the typical hexagonal or triangular islands observed in homo-epitaxy on the (111) plane of fcc metals. This anomalous growth mode shows a strong dependence on the coverage of the surfactant and hence demonstrates the possibility of using the surfactant coverage as a useful control parameter in fine-tuning the shape and aspect ratio for the growth of metal nanorods. The Au sheet grows preferentially in the $< 11\bar{2} >$ direction and its width changes in a quantized manner in steps of $6.5a$ (~1.85 nm) where a is the nearest neighbor distance for Au atoms. This unexpected symmetry-breaking growth mode is proposed to arise from the interaction between the edges of the growing Au sheet and the OT overlayer which behaves as a molecular carpet covering both the Au(111) substrate and the Au sheet. The growth of the Au sheet deforms the molecular carpet. Due to the crystalline structure of the OT layer, the energy involved in distorting the molecular carpet is directionally anisotropic. This hinders the growth of the Au sheet in certain directions leading to symmetry-breaking growth.

Key words: Symmetry breaking growth; two-dimensional materials; Gold nano-sheets; self-assembly; nucleation and growth; scanning tunneling microscopy.

Metal nano-particles have become an important family of novel materials due to their wide range of technological applications.[1-5] Gold nanorods in particular are attracting a high level of attention due to their multiple plasmonic modes (transverse and longitudinal plasmons) within the UV-vis-NIR absorption spectrum.[6] Although a number of synthetic methods have been successfully developed for producing Au nanorods, there remain great challenges in accurate control over the shape and aspect ratio of the rods. A thorough understanding of the detailed mechanism of nanorod formation and the atomic structure of the nanorods is essential in refining the synthesis procedure.

The most favored route for Au nanorod formation involves wet chemistry using surfactant such as cetyltrime-

thylammonuim briomide (CTAB).[7] The wet chemical environment makes it difficult to perform *in situ* characterization of the nanorods during growth. For instance, the structure of the nanorods is analyzed by performing *ex-situ* microscopic imaging and electron diffraction.[8] A striking feature in nanorod synthesis is the pronounced anisotropic growth, and it has been suggested that the different adsorption energies of CTAB on different crystal faces of Au are at least partially responsible for this unidirectional growth.[8,9] Here we report the anisotropic growth of single-atomic-layer and bilayer gold nano-sheets on the (111) plane of gold in the presence of a sub-monolayer of octanethiol (OT) surfactant in vacuum. We demonstrate that the growth of the Au sheet is greatly affected by the surface coverage of OT. Under the optimum surface coverage, we observed anisotropic growth of long rectangular Au sheets with the $< 11\bar{2} >$ axis as the preferred growth direction. Although alkanethiols have long been the popular agent for the synthesis and passivation of Au nanoparticles,[10,11] they have hardly been used in the synthesis of Au nanorods. Our findings indicate that Au nanorods can be synthesized using alkanethiol as the capping agent if the appropriate coverage can be maintained during growth. The growth condition in our study is rather different from that in wet chemistry. However, the way the surfactant molecules interact with the Au surface and the effect of the surfactant in controlling the growth mode is rather similar to that in wet chemistry synthesis of Au nanorods. Moreover, *in situ* scanning tunneling microscopy (STM) imaging provides direct information for identifying the growth mechanism.

The octanethiol monolayer is prepared using the standard approach[12,13] by immersing the Au sample into a 1 mM octanethiol/ethanol solution. The sample after drying in air is transferred into an ultra-high vacuum (UHV) system where all the experiments are conducted. Au atoms are deposited under UHV conditions at room temperature from a physical vapor deposition source. When Au atoms land onto the OT covered Au(111), the atoms "sink" to the thiol/Au(111) interface where they diffuse laterally and aggregate into single-atomic-layer Au islands. The Au islands are thus sandwiched between the Au(111) substrate and the OT layer. The maximum coverage of OT on Au(111) is 1/3 monolayer (ML) corresponding to one molecule for every three Au atoms.[12,13] A number of different structural phases exist for alkanethiol SAMs on Au(111)[14] at less than full coverage and these phases can be achieved by removing molecules via partial thermal desorption.

Figure 1(a) shows a simple ball model illustrating the formation of single atomic layer metal islands on the (111) plane of fcc metals. The herringbone reconstruction of the Au(111) surface is not shown for simplicity. Under normal conditions, the Au(111) substrate with its three-fold symmetry naturally favors the formation of single layer Au islands with hexagonal or triangular shapes,[15] as required by the minimization of the Gibbs free energy. The three edges of the triangle in the ball model are type-B steps exhibiting (111) micro-facets. A rectangular island with ex-

posed $[11\bar{2}]$ step edges is also shown in Fig. 1(a). Such kind of islands are unstable due to the excessive amount of energy associated with the $[11\bar{2}]$ oriented steps and as a matter of fact they have never been observed in homoepitaxy on the (111) plane of fcc metals.

Fig. 1(b) shows an STM image of triangular shaped Au islands formed on Au(111) in the presence of ~0.2 ML of OT. The herringbone reconstruction of Au(111) is completely lifted due to the adsorption of OT. All the triangular islands have the same azimuthal orientation, and this is consistent with the structural model of the triangular island in Fig. 1(a). The structure of the OT layer, visible in the background in Fig. 1(c), is made of short segments of RS-Au-SR rows aligned in the $[11\bar{2}]$ direction.[16-17] A schematic diagram of the RS-Au-SR staple rows can be found in the Supplement Information[18] which consists also of high-resolution STM images showing individually resolved RS-Au-SR units. Each segment of RS-Au-SR row in Fig. 1(c) contains ~ 3 to 5 RS-Au-SR. The triangular Au islands are also covered by RS-Au-SR, although no regular packing structure of RS-Au-SR is observed on the islands. This is probably due to the small size of the islands. We will show more clearly later with the rectangular Au nano-sheets that the Au sheets are indeed covered by OT of the same coverage as that on the Au(111) substrate. We did not deposit Au onto the clean Au(111) at RT because no stable Au islands can form at RT in the absence of OT. Deposited Au atoms would diffuse to existing step edges rather than forming new islands. At low sample temperatures, small Au islands with irregular shapes can form at the elbow sites on Au(111).[19]

The shape of the Au islands seen in Fig. 1(c) is expected for homoepitaxy on the (111) plane of the fcc metals. The presence of OT is simply to lift the herringbone reconstruction and modify the surface energy of the Au island. What came as a surprise was the discovery of rectangular Au islands on the same sample surface, Fig. 1(d). These rectangular Au sheets are single atom high, ~ 5 nm wide and up to ~ 50 nm long. Strictly speaking, the shape is not rectangular as one end appears to be curved. In Fig. 1(e), the straight rows of RS-Au-SR staples can be seen on both the Au(111) substrate and the newly formed Au nano-sheets. Thus, the Au islands are covered by OT and the structure of the OT layer on top of the Au islands is the same as that on the Au(111) substrate. The coverage of OT corresponding to the image in Fig. 1(c) is slightly lower than that corresponding to the image in Fig. 1(e) because thermal desorption leads to gradual breaking up of the long rows into short segments. On the same sample, domains with long straight rows and domains with short segments of staggered rows are often found sit next to each other and the two structures can interchange. What interesting is that Au islands inside the straight row domain are rectangular in shape whilst inside the short-segmented-row domain they are triangular. An immediate question to be answered is what controls the shape of the Au island?
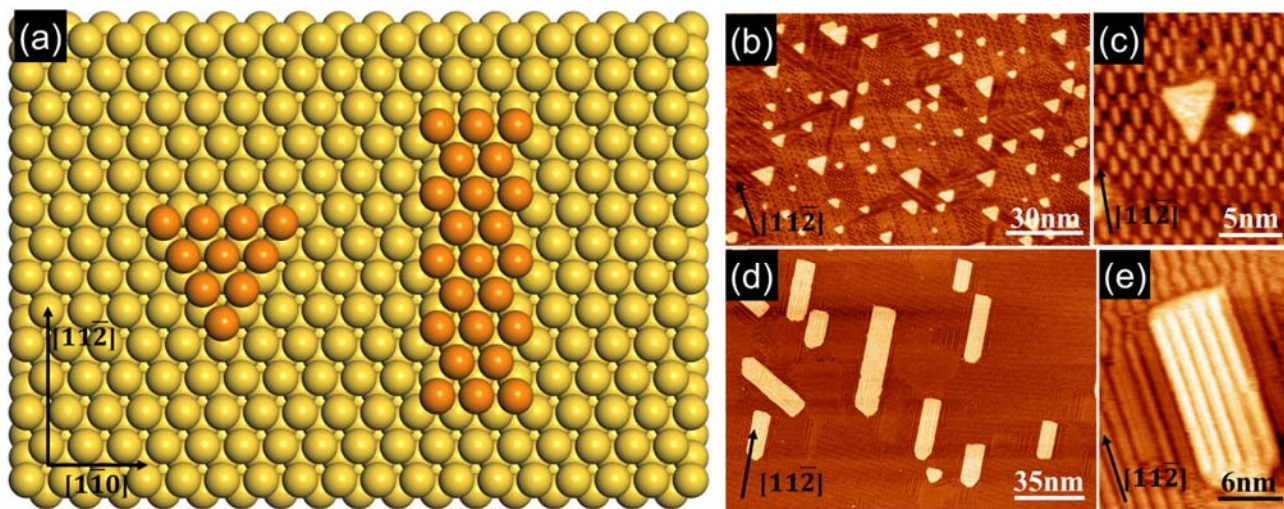
Figure 1. (a) Ball model of single atomic layer islands on the (111) plane of fcc metals. The triangular island is expected to be the stable geometric shape at room temperature where all the step edges consist of close-packed atoms and belong to the type-B step. The rectangular island with its long axis parallel to the [$11\bar{2}$] direction is unstable because of the high step energy associated with the [$11\bar{2}$] oriented steps. This type of rectangular islands has not been observed on the (111) plane of fcc metals. (b) STM image of triangular gold islands formed on Au(111) in the presence of 0.2 ML of OT, after deposition of 0.18 ML of Au atoms at RT. All the triangular islands have the same azimuthal orientation suggesting that the three step edges of each triangle are the same type. (c) OT in the form of staggered RS-Au-SR rows running parallel to the [$11\bar{2}$] direction. RS-Au-SR staples covering the surface of the triangular islands are in a two-dimensional gas state. (d) STM image of "rectangular" Au islands observed on the same sample, in regions where long straight RS-Au-SR rows are observed. (e) The same striped-phase of OT is found on the Au(111) substrate as well as on top of the Au island.

The shape of metal islands grown on various crystal planes of fcc metals has been extensively studied.[15, 20-22] The nucleation and growth of atomic islands are governed by the energies of atomic steps and are usually closely related to the symmetry of the substrate. Thus, on the (100) plane of fcc metals, the islands have a square shape;[21] on the (110) plane, they have a rectangular shape;[22] and on the (111) plane, they have either a triangular or a truncated triangular shape.[20] Using surfactant molecules can alter surface and step energies leading to modified island shapes. For instance, in the synthesis of Au nanorods from wet chemistry, selective passivation of crystal faces by CTAB is believed to be a key factor for controlling the shape of the rods.[8] Adsorption of OT onto the [$11\bar{2}$] step might cause a significant reduction of the step energy and hence makes the [$11\bar{2}$] step more stable than the [$1\bar{1}0$] step. However, this step passivation mechanism does not explain our observations. The triangular and rectangular islands are observed on the same sample under the same experimental conditions. Hence, if step passivation were responsible for the island shape, we would expect either triangular or rectangular island, but not both. Our observation suggests that the structure of the OT capping layer on

the Au(111) has a major influence on the shape of the Au island. Here we want to compare with Au(111) covered with ethylthiolate, $(CH_3CH_2)S$-Au-$S(CH_2CH_3)$ also in the striped phase with long staple rows.[23] Figure 2 shows several Au islands observed on Au(111) after deposition of Au onto ethylthiolate covered Au(111). Here we can clearly see the $(CH_3CH_2)S$-Au-$S(CH_2CH_3)$ rows on both the Au(111) substrate and on top of the Au islands. The Au islands here appear to have rounded edges without the distinctive rectangular geometry. There is no evidence of preferred growth in the direction of the staple rows. This is one further piece of evidence that the formation of rectangular Au islands is not a simple result of step passivation because ethanethiol is expected to be just as effective as octanethiol for passivation of the steps.

The difference in island geometry hence points to the role of the alkane chains in the thiol. As the chain length increases, the van der Waals interaction becomes more significant and expected to play a more important role in the growth of the Au island. When a layer of Au islands is inserted into the OT/Au(111) interface, the OT layer is disrupted as shown schematically in Fig. 2(b) where two neighboring rows of RS-Au-SR are displayed. The row on the right is lifted up by the Au island while the left row sits

on the Au(111) substrate, creating a boundary within the OT layer. The boundary, highlighted with a green dashed line, has a specific boundary energy γ_{VDW}. VDW here signifies that the boundary energy originates from the van der Waals interaction between the alkane chains. The Au step has specific step energy γ_{Au}. The stability of the whole system can be evaluated with $\gamma_E = \gamma_{Au} + \gamma_{vdw}$. γ_{VDW} is usually neglected in systems where γ_{VDW} is much lower than γ_{Au}. However, for the system studied here, γ_{VDW} becomes an important parameter and it cannot be ignored when the stability of the Au island is considered.

The step energy, γ_{Au}, depends on the crystallographic orientation of the step. The boundary energy, γ_{VDW}, is also a function of azimuthal direction because the OT layer has its own crystalline structure with a particular symmetry. It is possible that the two energies have the same directional dependence, but in general, they are more likely to have different directional dependence. For example, the $[1\bar{1}0]$ oriented step is supposed to be the lowest energy step for atomic islands on Au(111), but a $[1\bar{1}0]$ oriented boundary within the OT layer is not necessarily the lowest energy boundary. The competition between γ_{Au} and γ_{VDW} decides the final shape of the Au island. In fact, if γ_{VDW} is greater than γ_{Au}, the shape of the island is mostly controlled by the boundary energy of OT, which can lead to anomalous island shapes. We can define $\gamma_E = \gamma_{Au} + \gamma_{vdw}$ as the effective step energy.

The step edge of the Au island in Fig. 2(b) at the boundary is a $[11\bar{2}]$ step which has a high γ_{Au}. Such a high γ_{Au} step becomes the dominant step edge of the observed Au islands suggesting that the boundary created within the OT layer has a low γ_{VDW}. The lateral distance in the $[1\bar{1}0]$ direction between the RS-Au-SR rows on each side of the boundary affects the van der Waals interaction between the two rows. In Fig. 2(b), each of the two rows is placed on the surface according to their normal arrangement. The distance between the alkane chain from the left of the boundary (the right arm of the row on the lower terrace) and that from the right side of the boundary (the left arm of the row on the upper terrace) is ~ 0.45 nm. This is roughly the distance required to optimize the van der Waals interaction between parallel alkane chains. The boundary energy in this case is mainly due to the vertical height offset of the two chains. It is also interesting to see that the $[11\bar{2}]$ direction is the close-packing direction of the RS-Au-SR staples. Thus, one may consider that the $[11\bar{2}]$ oriented boundary is the natural low γ_{VDW} boundary. Without a detailed evaluation of γ_{VDW} using DFT calculations, we are yet not ready to quantify the stability of the boundaries.

We will show later that the rectangular Au island can grow sideways by becoming wider, but the sideway growth is significantly hindered by the structure of the staple rows. As shown in Fig. 2(b), the expansion of the Au islands towards the left has an energy barrier which is needed to lift a whole row of RS-Au-SR staples. Breaking the staple row

or breaking an individual staple requires extra energy. For this reason, sideway growth is slow and shows a "quantized" behavior as the width increases in steps of a fixed distance. Based on the above discussion, we conclude that the formation of rectangular Au islands on Au(111) is a direct consequence of minimization of the boundary energy of the OT layer during the growth of the Au island. For the striped phase of the OT, the $[11\bar{2}]$ step of the Au island causes the least disturbance of the OT by allowing two RS-Au-SR rows, one on each side of the step, to maintain effective van der Waals interaction. The minimization of the boundary energy thus overcompensates for the high step energy of the $[11\bar{2}]$ step of Au.

The above discussion involving $\gamma_E = \gamma_{Au} + \gamma_{vdw}$ can also be applied to explain the Au islands of other geometric shapes. Figure 3(a) shows triangular islands found on the Au(111) surface in the presence of OT. The OT layer in this case consists of a rather regular array of short segments of RS-Au-SR rows. The blue and white triangles overlaid onto the image, as well as the schematic diagram in Fig. 3(b), demonstrate how the triangular island grows while maintaining the same type of boundaries. Although there are thiol molecules on top of the triangular islands, no regular structure is observed on the islands. This indicates a poor positional match between molecules on either side of the Au step, and hence a high boundary energy. The step edges of the triangular island are all aligned with the close-packing directions of Au atoms. Therefore, the triangular islands are examples of high γ_{VDW} and low γ_{Au}. According to the scheme of Fig. 3(b), triangular islands can expand as long as the edges of the islands are properly located so to avoid "cutting through" the staple rows.

The most dense phase of the OT monolayer has the well-known $3 \times 2\sqrt{3} - \text{rect.}$ phase.[12,13] When Au is deposited onto this dense monolayer, the Au islands formed do not show any regular shape. The step edges of the island appear curvy, Fig. 3(c). The irregular shape of the Au islands came as a surprise considering that the $3 \times 2\sqrt{3} - \text{rect.}$ phase of the OT SAM has a high degree of ordering. By examining the detailed structure of the $3 \times 2\sqrt{3} - \text{rect}$ phase, Fig. 3(d), it becomes immediately clear why such a dense phase prevents the Au island from taking up a regular shape. The solid green line in Fig. 3(d) indicates a natural low energy boundary for the SAM. This line is parallel to the $[11\bar{2}]$ direction. Thus, a Au island can have one of its step edges parallel to this direction. The other two equivalent $<11\bar{2}>$ directions, marked by dashed green lines which can be seen to cut through the molecules, do not form natural boundaries for the OT. In Fig. 3(d), one can also find that the $<1\bar{1}0>$ directions, dashed red lines, are also not the directions for natural boundaries. In Fig. 3(c), each Au island has just one short straight step edge, indicated by the solid green line. These straight steps are $[11\bar{2}]$ steps. The rest of the step edges do not align to any particular crystallographic directions and appear curved.
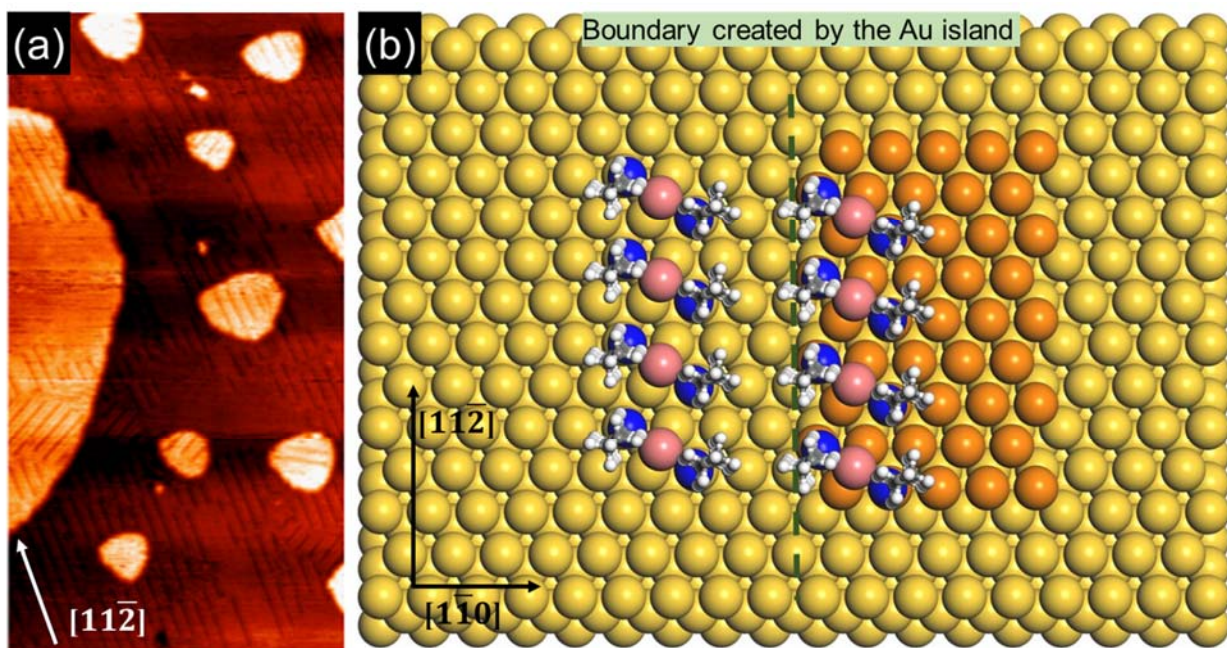
Figure 2. (a) STM image, 60 nm x 130 nm, showing Au islands formed on an ethanethiol covered Au(111). The ethanethiol is in its striped phase. The Au islands do not show the long rectangular shape as found on octanethiol-covered surface. There is no indication of preferred growth along the [$11\bar{2}$] direction. (b) Ball model illustrating the relationship between two RS-Au-SR rows, one on the upper terrace and the other on the lower terrace. The two rows are able to keep an optimal distance so that the alkane chains from the two rows can interact effectively. The blue colored spheres indicate the S atoms. Gray spheres and white spheres represent carbon and hydrogen, respectively. Pink spheres are the Au atoms within the RS-Au-SR staple. The dashed green line shows the boundary within the OT, created by the Au island.
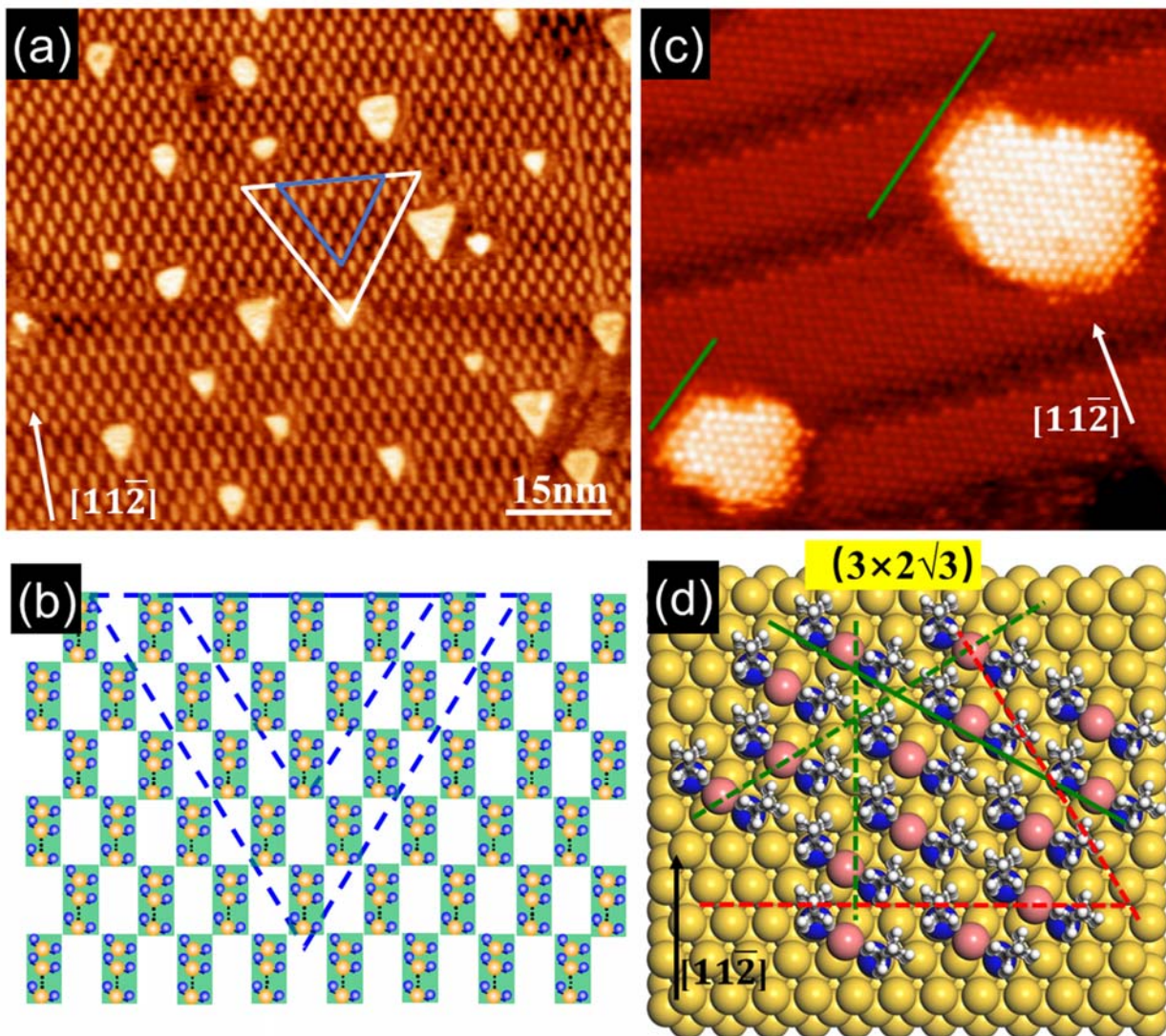
Figure 3. (a) STM image showing triangular gold islands on Au(111) covered by 0.2 ML of OT consisting of staggered short segments of staple rows. (b) Schematic diagram illustrating how the triangular islands expands while keeping the same type of step edges. The edges of the island avoid cutting through the staple rows. (c) Irregular shaped Au islands found inside the most-dense phase of OT monolayer. The green lines highlight the only straight step edges for these islands. (d) Ball model of the dense-phase of OT monolayer. The alkane chains appear to be close-packed when viewed from above, and this dense phase was initially called $\sqrt{3} \times \sqrt{3} - R30$ by mistake. The directions highlighted with green and red colored dashed lines are incompatible with the directions of low boundary energy for the OT layer. The solid green line shows a low-boundary-energy direction parallel to one of the <$11\bar{2}$> axes. The close-packing directions of gold, red-dashed lines, can be seen to be incompatible with the directions of natural boundaries of OT.
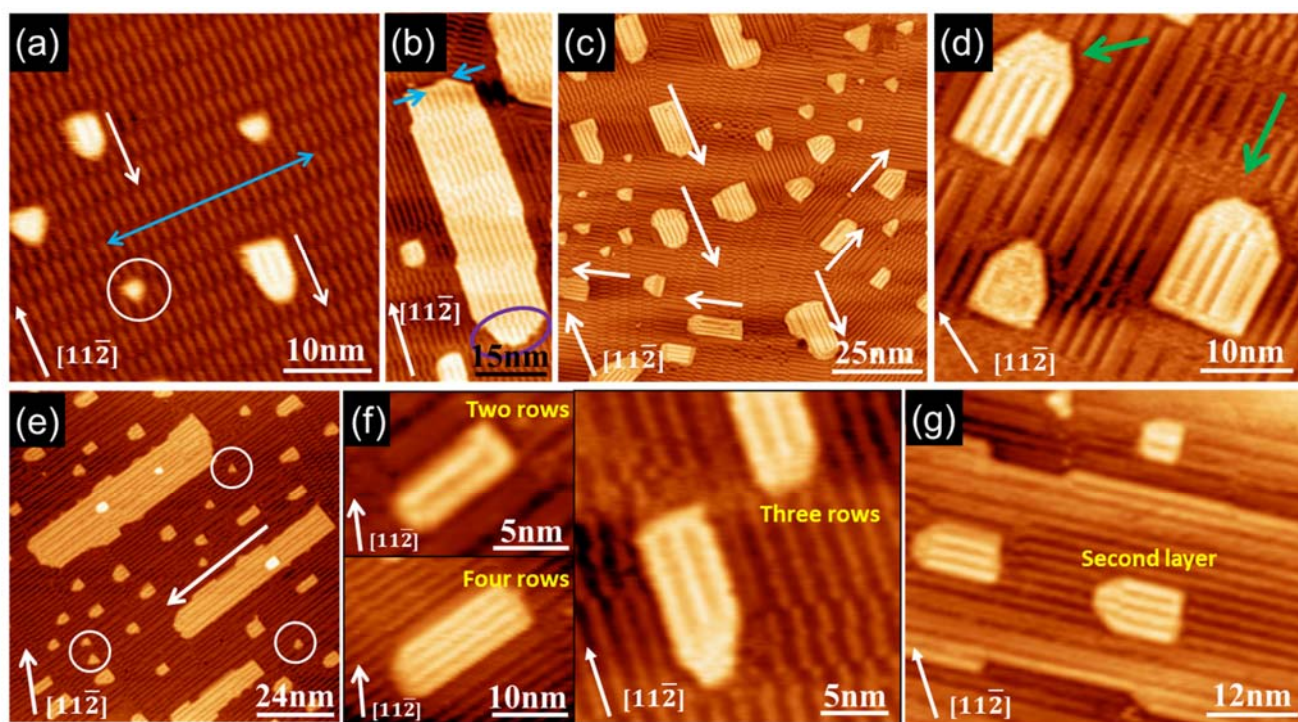
6

Figure 4. (a) Au islands are preferentially nucleated at defect sites such as domain boundaries. The double-headed blue arrow points to a row of defects due to the offset of the staple rows. White arrows indicate the direction of growth. (b) The rectangular island has a preferential growth direction. On end of the rectangle is pinned and immobile. This end has a straight [$1\bar{1}0$] oriented step. The lower end of the rectangle inside the purple oval is the growth front of the island. (c) Each island is oriented in such a way that its long axis is parallel to the stripes on Au(111). (d) The growing end of the island seems to be covered by thiol molecules in a disordered state. (e) The formation of second layer Au islands. The small islands are formed after a second round deposition of Au. (f) "Quantized" sideway expansion of the Au island. (g) Second layer islands on top of a large rectangular first layer island.

After establishing the mechanism for shape control of gold islands by thiol molecules, we now move on to discuss the growth process of the rectangular islands. The initial nucleation of the island occurs mostly at defect sites. For example, the boundary between two domains of striped phases as indicated by the double-headed blue arrow, Fig. 4(a). The initial nucleus has a triangular shape which gradually changes into a bullet shape due to anisotropic growth. The pointed end of the bullet grows in the direction pointed by the white arrows. The other end of the bullet appears to be pinned and hence unable to move at RT. Fig. 4(b) shows clear differences between the two ends of the rectangle. The pinned end has a straight atomic step. This step consists of close-packed Au atoms. We are unable to determine whether this is a type-A or a type-B step. However, it is expected that the difference in energetics between the two types of close-packed steps is responsible for unidirectional growth. Fig. 4(c) shows a number of rectangular islands. Each island has its long axis parallel to one of the

<$11\bar{2}$> directions. The direction of stripes on top of the island is always parallel to the direction of the stripes on the Au(111) substrate, in the immediate vicinity of the islands. This is consistent with the conclusion we made earlier that the shape of the island is controlled by the structure of the SAM on the Au(111) substrate, through the van der Waals interaction among the alkane chains.

In Fig. 4(d), it can be seen that the growing end of the rectangle has a small area covered by disordered thiols. This disordered molecular patch suggests that this area is still moving towards equilibrium. Fig. 4(e) shows large and small rectangular islands. The large ones are formed after thermal annealing to 328 K. The small islands are formed after another round of deposition. For the newly formed Au islands, there is a minimum width that supports two bright rows of molecules: one row at each edge of the island. From this minimum width of two bright rows, the island can expand sideways to a width that supports three bright rows: one at each edge with an extra one in the middle, Fig.

7

4(f). Therefore, the width of the rod increases in steps of 1.85 nm which is the period of the stripes in the $[1\bar{1}0]$ direction. 1.85 nm is close to *6.5a* where *a* is the nearest neighbor distance of gold atoms. Fig. 4(g) shows the formation of second layer Au islands on top of a large rectangular island. It can be seen that the second layer follows the same growth mode. Therefore, by adding gold to an existing rectangular sheet, multilayer sheets resembling of Au nanorods could be formed.

The anisotropic growth of Au islands leads to an increased aspect ratio with the area of the island. Figure 5 gives a plot of the length over width ratio of the single layer Au nano-sheets as a function of the area of the rods. As can be seen, the ratio increases with the size of islands. This is a direct consequence that the longitudinal growth is significantly faster than the transvers growth. It implies the energy barrier for sideway expansion of the Au islands remains constant. Therefore, very high aspect ratio can be achieved for large sheets.
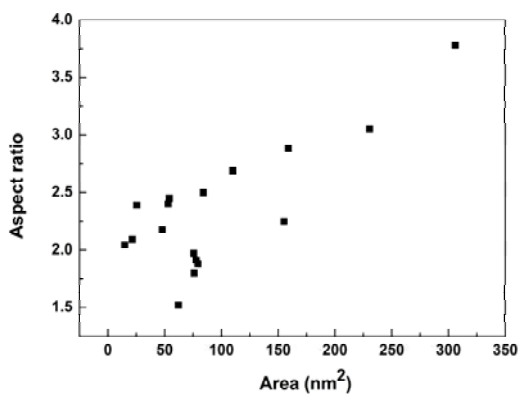

Figure 5. Aspect ratio (length/width) of the Au nano-sheet plotted as a function of the size (area) of the sheet. The length is measured along the $<11\bar{2}>$ directions and the width is measured along the orthogonal $<1\bar{1}0>$ directions.

Shape selectivity is an important issue in nanorod synthesis. Here for the single layer of Au nano-sheets, accurate shape control can be achieved by using OT with the appropriate coverage and structure. The OT layer can have several phases on Au(111) and it is not easy to prepare a single phase over the whole sample except for the maximum coverage phase. However, by slow thermal annealing for a long enough time and minimizing temperature gradient across the sample, it is possible to produce large single-phase domains. Figure 6 shows that within a single-phase domain, shape selectivity can reach nearly 100%.
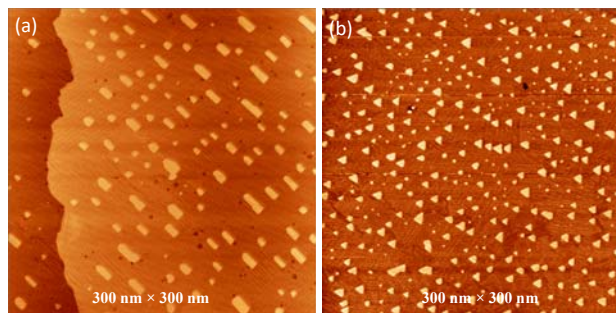

Figure 6. STM images showing ~100% rectangular Au nano-sheets within a single domain in (a), and ~100% triangular island in another domain in (b).

In summary, we have successfully grown single atomic layer and bi-layer rectangular gold sheets, with high aspect ratios, on a (111) plane of an fcc metal by breaking the symmetry constraint of the substrate. The width of the sheets is found to increase in a quantized manner with the minimum discrete increment of *6.5a*. This anomalous growth arises from the force field of a capping molecular layer of octanethiols. Our findings demonstrate the importance of a structured surfactant in controlling the shape of nano-crystals. For the same surfactant, its surface coverage and hence structure can provide varied energy barriers for guiding the anisotropic growth of nano-scale materials. The Au nano-sheets produced on the Au(111) substrate are not expected to have interesting plasmonic properties due to the strong coupling to the bulk metal. However, the growth mechanism that we have discovered is highly relevant to shape-controlled synthesis of nano-particles.

Methods. The gold substrate is prepared by physical vapor deposition of Au onto highly oriented pyrolitic graphite (HOPG). The thickness of the gold film is ~ 300 nm and the surface preferentially shows the (111) crystal plane. The OT monolayer is deposited onto the Au substrate by immersing the sample in 1 mM octanetiol/ethanol solution for 24 hours. The sample is then thoroughly rinsed with pure ethanol and dried in air before transferring into the UHV system. In vacuum thermal annealing is performed to reduce the coverage of OT to an appropriate level before Au is deposited using a high temperature Knudsen cell. All STM imaging is conducted using an Omicron Fermi STM. Electrochemically polished tungsten tips are used.

ASSOCIATED CONTENT

Supplementary Information

The Supplementary Information contains structural models of the striped octanethiol monolayer and additional STM images.

AUTHOR INFORMATION

Corresponding Authors

*E-mail: Prof. L. Chi, email: chilf@suda.edu.cn, Dr. M Pan, minghupan@hust.edu.cn and Dr. Q Guo, Q.Guo@bham.ac.uk.

Author Contributions

All authors contributed to data analysis and writing of the manuscript. X Zhang, Y Wang, T Zhao, H Bai, H Ding and X Qin performed experiments.

Notes

The authors declare no competing financial interest.

REFERENCES

[1] Dong, Q.; Wang, X.; Hu, X.; Xiao, L.; Zhang, L.; Song, L.; Xu, M.; Zou, Y.; Chen, L.; Chen, Z.; Tan, W. *Angew. Chem. Int. Ed.* **2018**, *57*, 177-181.

[2] Maioli, P.; Stoll, T.; Sauceda, H. E.; Valencia, I.; Demessence, A.; Bertorelle, F.; Crut, A.; Vallee, F.; Garzon, I. L.; Cerullo, G.; Del Fatti, N. *Nano Lett.* **2018**, *18*, 6842-6849.

[3] Zhang, Z.; Wang, L.; Wang, J.; Jiang, X.; Li, X.; Hu, Z.; Ji, Y.; Wu, X.; Chen, C. *Adv. Mater.* **2012**, *24*, 1418-1423.

[4] Quiroz, J.; Barbosa, E. C. M.; Araujo, T. P.; Fiorio, J. L.; Wang, Y. C.; Zou, Y. C.; Mou, T.; Alves, T. V.; de Oliveira, D. C.; Wang, B.; Haigh, S. J.; Rossi, L. M.; Camargo, P. H. C. *Nano Lett.* **2018**, *18*, 7289-7297.

[5] Matsuhisa, N.; Inoue, D.; Zalar, P.; Jin, H.; Matsuba, Y.; Itoh, A.; Yokota, T.; Hashizume, D.; Someya, T. *Nat. Mater.* **2017**, *16*, 834-840.

[6] Fu, L.; Liu, Y.; Wang, W.; Wang, M.; Bai, Y.; Chronister, E. L.; Zhen, L.; Yin, Y. *Nanoscale* **2015**, *7*, 14483.

[7] Jana, N. R.; Gearheart, L.; Murphy, C. J. *J. Phys. Chem. B* **2001**, *105*, 4065.

[8] Johnson, C. J.; Dujardin, E.; Davis, S. A.; Murphys, C. J.; Mann, S. *J. Mater. Chem.* **2002**, *12*, 1765-1770.

[9] Meena, S. K.; Sulpizi, M. *Angew. Chem. Int. Ed.* **2016**, *55*, 11960-11964.

[10] Brust, M.; Fink, J.; Bethell, D.; Schiffrin, D. *J. Chem. Soc. Commun*. **1995**, *16*, 1655-1656.

[11] Sardar, R.; Shumaker-Parry, J. S. *J. Am. Chem. Soc.* **2011**, *133*, 8179-8190.

[12] Love, J. C.; Estroff, L. A.; Kriebel, J. K.; Nuzzo, R. G.; Whitesides, G. M. *Chem. Rev.* **2005**, *105*, 1103-1170.

[13] Guo, Q.; Li, F-S. *Phys. Chem. Chem. Phys*. **2014**, *16*, 19074-19090.

[14] Poirier, G. E. *Langmuir* **1999**, *15*, 1167-1175.

[15] Cox, E.; Li, M.; Chung, P-W.; Ghosh, C.; Rahman, T.; Jenks, C. J.; Evans, J. W.; Thiel, P. A. *Phys. Rev. B* **2005**, *71*, 115414.

[16] Jadzinsky, P. D.; Calero, G.; Ackerson, C. J.; Bushnell, D. A.; Kornberg, R. D. *Science*, **2007**, *318*, 430-433.

[17] Hakkinen, H. *Nature Chem.* **2012**, *4*, 443-455.

[18] Supplement Information.

[19] Rokni-Fard, M.; Guo, Q. *J. Phys. Chem. C* **2018**, *122*, 7801-7805.

[20] Ovesson, S.; Bogicevic, A.; Lundqvist, B. I. *Phys. Rev. Lett*. **1999**, *83*, 2608.

[21] Linderoth, T. R.; Mortensen, J. J.; Jacobsen, K. W.; Lægsgaard, E.; Stensgaard, I.; and Besenbacher, F. *Phys. Rev. Lett.* **1996**, *77*, 87.

[22] De Giorgi, C.; Aihemaiti, P.; De Mongeot, F. B.; Boragno, C.; Ferrando, R.; and Valbusa, U. *Surf. Sci*. **2001**, *487*, 49-54.

[23] Li, F.; Tang, L.; Voznyy, O.; Gao, J.; Guo, Q. *J. Chem. Phys*. **2013**, *138*, 194707.

TOC Graphic

Single-Atomic-Layer Au Nanorod

10 nm